

# A Consideration of Bidirectional Superposed Dual Active Bridge DC-DC Converter

Toshiro Hirose<sup>\*,\*\*</sup> and Hirofumi Matsuo<sup>\*\*</sup>

<sup>\*</sup> Nishimu Electronics Industries Co., Ltd, Saga, 842-0032, Japan

<sup>\*\*</sup> Nagasaki University, Nagasaki, 852-8521, Japan

**Abstract**— This paper describes the principles and characteristics of a novel bidirectional superposed dual active bridge dc-dc converter with an ac-link transformer, which has a mechanism formed from two bridge-type converters that are linked through superposition in additive polarity in series. Conventionally, for an isolated dual active bridge dc-dc converter, the rated voltage of its switching elements is decided according to the dc power source voltage and load current. Therefore, as the voltage and current specifications of a dc-dc converter become higher, physical size becomes larger, conduction and switching losses increase and power efficiency reduces. To solve this problem, the authors devised the proposed dc-dc converter capable of lowering the rated voltage of switching elements, by means of sharing dc power source voltage and load current between two converters. Further, the capacity of the high frequency transformer becomes small, making the dc-dc converter more efficient and smaller. We designed and constructed a 1kW dc-dc converter prototype, and conducted performance evaluation testing. As a result, a conversion efficiency of 96.6% at a rated output of 1kW was obtained. A detailed analysis of power flow was also carried out, to identify the characteristics of the converter developed.

**Index Terms**—bidirectional dc-dc converter, superposed dual active bridge, ac-link transformer, ZVS/ZVC.

## I. INTRODUCTION

For isolated dual active bridge dc-dc converters which have been previously researched, various techniques to improve converter conversion efficiency have been applied: for instance, application of resonant type converter using snubber capacitance[1], uses of silicon carbide (SiC) power devices and new magnetic materials[2]. And isolated dual active bridge dc-dc converter have been applied for use in hybrid electric vehicles[3] and energy storage systems[4]. Power generation systems incorporating natural energy are generally equipped with secondary batteries and electric double-layer capacitors; and to control their charge/discharge operation, bidirectional dc-dc converters have also been widely employed[5].

As for this research, a gratitude is given to Mr. H. Yoshimoto with Nishimu Electronics Industries Co., Ltd..

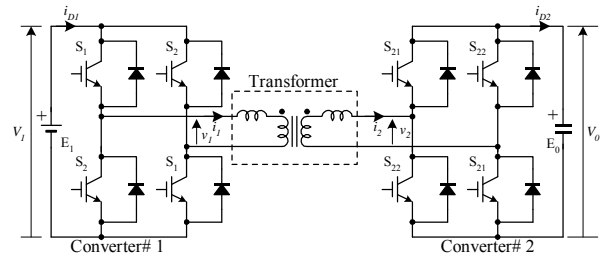


Fig. 1. Bidirectional isolated dual active bridge dc-dc converter .

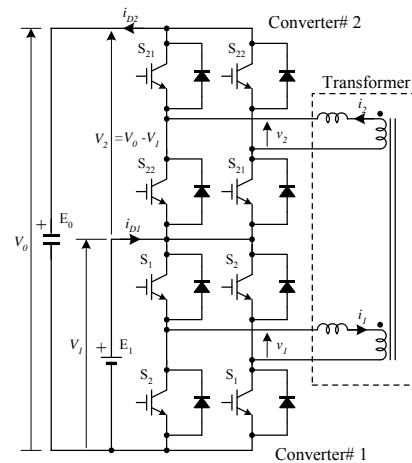


Fig. 2. Novel superposed dual active bridge dc-dc converter with an ac-link transformer.

In the pursuit of high energy efficiency for such equipment, bus voltage tends to be high along with development of high-tech switching devices, while in practical terms energy storage devices such as Li-ion batteries and electric double-layer capacitors cannot meet the high voltage requirements. Therefore, in the case that high voltage, high current specifications are required, dc-dc converters need to be large in size, resulting in a reduction in power efficiency due to an increase in conduction and switching losses. As a solution to this problem, the authors proposed a bidirectional superposed dual active bridge dc-dc converter. The proposed converter, which has a mechanism formed from two bridge-type converters that are linked through superposition in additive polarity in series, is capable of lowering the rated voltage of switching elements, by means of sharing dc power source voltage and load current at the high-voltage side between the two converters[6]. Fig.1 shows the circuit diagram of a conventional converter, and Fig.2 shows the circuit

diagram of our proposed dc-dc converter. In Fig.1, converter #1 is set on the low-voltage side, while converter #2 is set on the high-voltage side. The low-voltage side and high-voltage side are generally insulated; however, the conventional dc-dc converter has problems in that 1) the rated current of converter #1 switching elements are controlled by the converter AC current ( $i_i$ ), causing a high-current condition; and 2) the rated voltage of converter #2 switching elements are controlled by the voltage ( $V_o$ ) on the high-voltage side, causing a high-voltage condition.

In contrast, the proposed converter has no function to isolate the input and output power circuits; however, it has the following beneficial characteristics:

- 1) The output voltage ( $V_o$ ) of power source ( $E_o$ ) on the high-voltage side can be shared by converters #1 and #2 based on the transformer winding turns ratio. For instance, when the turns ratio is 1:1, the rated voltage of switching elements of converters #1 and #2 is half of  $V_o$ , contributing to the lowering of the switching element voltage rating.
- 2) The DC current ( $i_{D1}$ ) passing through power source ( $E_1$ ) on the low-voltage side can be shared by converters #1 and #2 based on the transformer winding turns ratio. For instance, when the turns ratio is 1:1, the rated current of switching elements of converters #1 and #2 is half of  $i_{D1}$ , contributing to the lowering of the switching element current rating.
- 3) Through mechanisms 1) and 2), the rated capacity to be processed by the transformer is decreased by half, contributing to downsizing as well as loss reduction.
- 4) Zero-current switching (ZCS) and zero-voltage switching (ZVS) are realized under a wide operation range when all switching elements are turned on, resulting in high efficiency.

## II. OPERATING MODES OF THE PROPOSED DC-DC CONVERTER

Figs.3 and 4 show AC output current waveforms at the time of dc-dc converter switching operation in power regenerative and running modes, respectively. An individual converter is driven in one-pulse mode without controlling pulse width. The on-duty ratio between S1 and S2, as well as that between S2 and S22, is 50%. To control output power in power running mode, the phase of AC terminal voltage ( $v_1$ ) of converter #1 advances against the phase of AC terminal voltage ( $v_2$ ) of converter #2. In contrast, to control output power in power regenerative mode, the phase of converter #1 lags behind that of converter #2. The phase control operated in Fig.2 is identical to that operated in Fig.1.

Depending on the magnitude of current transmitted, and voltage magnitudes of DC power sources ( $V_1$ ,  $V_2$ ), AC output currents ( $i_1$ ,  $i_2$ ) of dc-dc converter have three waveform patterns of current waveforms; that is, patterns (a), (b) and (c), as shown in Figs.3 and 4. In the case of pattern (c) in both power running and power regenerative modes, turn-on of all switching elements occurs under the

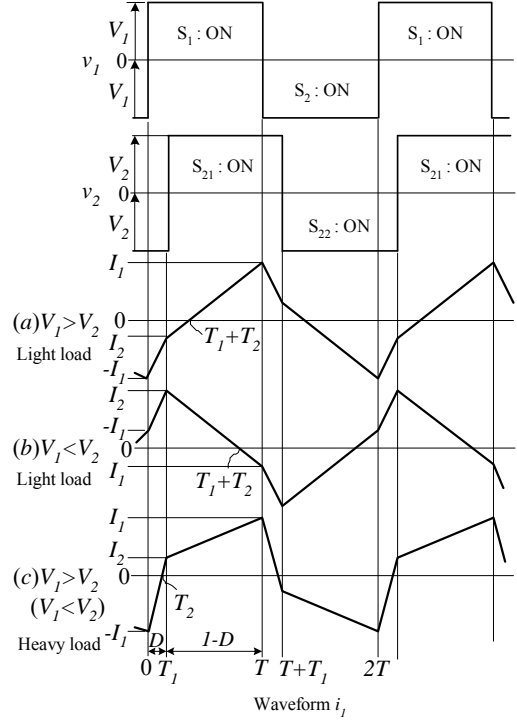


Fig. 3. Operating waveforms in power running mode.

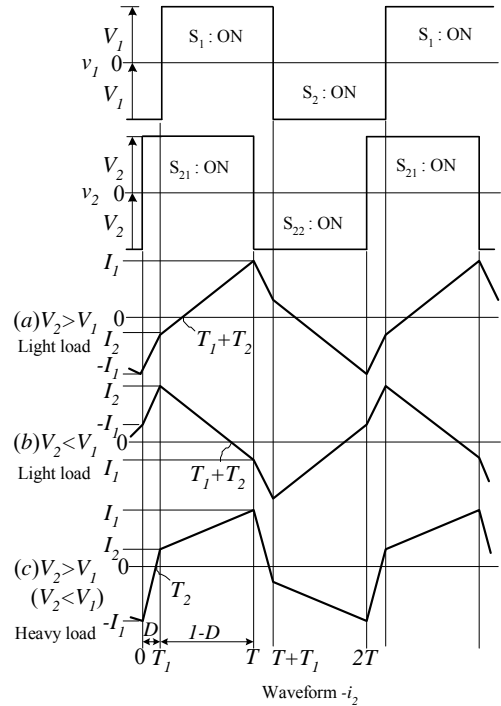


Fig. 4. Operating waveforms in regenerative mode.

condition of ZCS and ZVS, because the anti-parallel diode is in on-state. In contrast, the hard-turn-on phenomenon occurs in particular switching elements; that is, S21 and S22 in pattern (a), S1 and S2 in pattern (b) in power running mode, as well as S1 and S2 in pattern (a), S21 and S22 in pattern (b) in power regenerative mode. In this case, however, the current flowing to switching elements is small, resulting in only a minor switching loss.

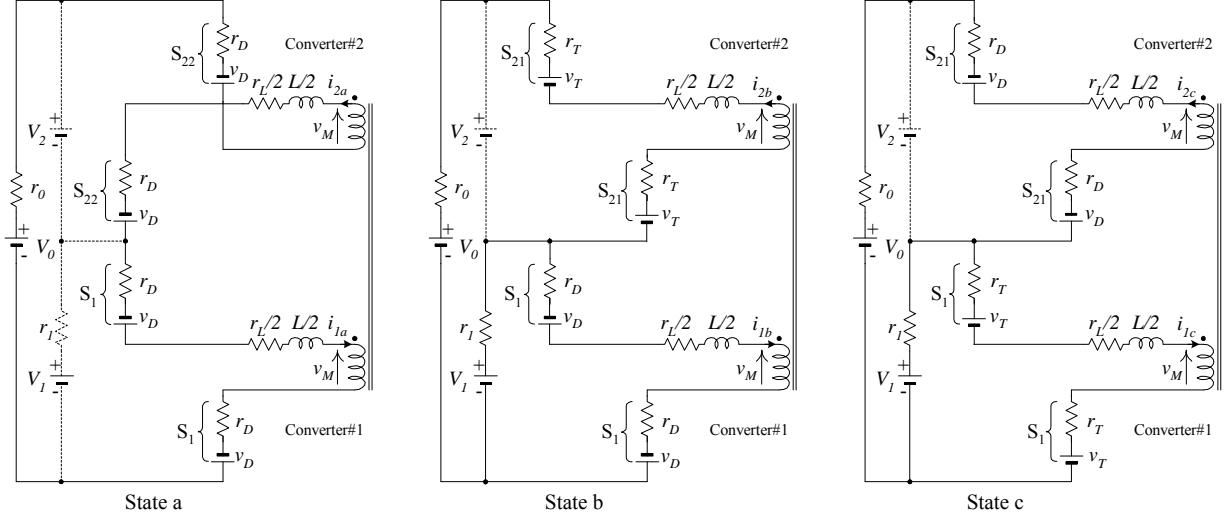


Fig. 5. Current-route and equivalent circuit.

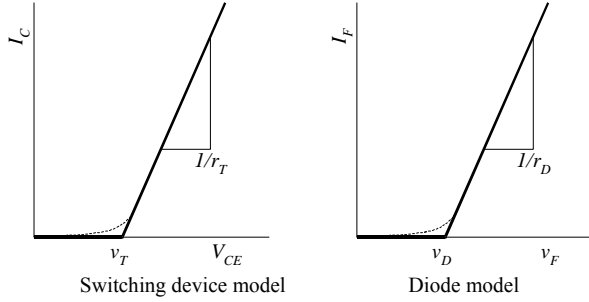


Fig. 6. Device models.

### III. OPERATING ANALYSIS

In the case of pattern (a) in power running mode, states that emerged in the time periods  $0 \sim T_1$ ,  $T_1 \sim T_1 + T_2$ ,  $T_1 + T_2 \sim T$  are defined as states a, b and c, respectively. To analyze power flow, we set up circuits equivalent to these states as shown in Fig.5, and obtained switching device and diode models by applying the method of approximation, as shown in Fig.6. Using the parameters of the converter circuit listed in Table 1, AC output waveform ( $i_j$ ) was obtained from numerical calculations.

#### A. State Analysis

##### 1) State a ( $t = 0 \sim T_1$ )

$S_1$  is turned on under the condition of  $i_{1a} = i_{2a} = -I_1$  when  $t = 0$ , and then state a starts. At this time, diodes in an anti-parallel connection with  $S_1$  are already in a turn-on condition. Since directions of current flows ( $i_{1a}$ ,  $i_{2a}$ ) do not change rapidly,  $i_{1a}$  flows to diodes of  $S_1$ , and  $i_{2a}$  flows to diodes of  $S_{22}$ . Current does not flow to  $V_1$ . The following two differential equations are given by the equivalent circuit of state a shown in Fig.5.

$$V_0 = r_0 i_{2a}(t) + 2r_D i_{2a}(t) - 2v_D + \frac{r_L}{2} i_{2a}(t) + \frac{L}{2} \frac{di}{dt} i_{2a}(t) - v_M(t) + V_1 \quad (1)$$

$$V_1 = 2r_D i_{1a}(t) - 2v_D + \frac{r_L}{2} i_{1a}(t) + \frac{L}{2} \frac{di}{dt} i_{1a}(t) + v_M(t) \quad (2)$$

Default values of  $i_{1a}$  and  $i_{2a}$  are set as  $-I_1$ . The Laplace transforms of both Eqs. (1) and (2) are used to obtain Eqs. (3) and (4).

$$\frac{V_0}{s} = \left( \frac{Ls + r_L}{2} + 2r_D + r_0 \right) I_{2a}(s) - \frac{2v_D}{s} + \frac{LI_1}{2} - V_M(s) + \frac{V_1}{s} \quad (3)$$

$$\frac{V_1}{s} = \left( \frac{Ls + r_L}{2} + 2r_D \right) I_{1a}(s) - \frac{2v_D}{s} + \frac{LI_1}{2} + V_M(s) \quad (4)$$

Since  $i_{1a} = i_{2a}$ , Eq. (5) is obtained from Eqs. (3) and (4).

$$I_{1a}(s) = I_{2a}(s) = \frac{V_0 + 4v_D - LI_1 s}{Ls \left( s + \frac{r_L + r_0 + 4r_D}{L} \right)} = \frac{\frac{V_{1a}}{r_a} - \frac{V_{1a}}{r_a} + I_1}{s + \frac{r_a}{L}} \quad (5)$$

Here, Eq. (6) is obtained from the following formulas:

$$r_a = r_L + r_0 + 4r_D, \quad V_{1a} = V_0 + 4v_D$$

$$i_{1a}(t) = i_{2a}(t) = \frac{V_{1a}}{r_a} - \left( \frac{V_{1a}}{r_a} + I_1 \right) e^{-\frac{r_a}{L} t} \quad (6)$$

Further, when the current is defined as  $I_2$  at time  $T_1$ , and  $T_1/T = D$ , Eq. (7) is obtained from Eq. (6).

$$e^{-\frac{\pi r_a D}{\omega L}} = \frac{\frac{V_{1a} - I_2}{r_a}}{\frac{V_{1a} + I_2}{r_a}} \quad (7)$$

## 2) State b ( $t = T_1 \sim T_1 + T_2$ )

$S_{21}$  is turned on when  $t = T_1$  after  $S_{22}$  is turned off, and reverse recovery current flows until the reverse recovery for diodes of  $S_{22}$  is completed, which causes DC power source ( $V_2$ ) to short-circuit. In this case, the hard-turn-on phenomenon of  $S_{21}$  occurs. However, this phenomenon emerges in the light load period, resulting in only a minor switching loss. In the case of pattern (c) in power running mode, when  $S_{21}$  is turned on under the condition that diodes of  $S_{21}$  are in a on-state, resulting in the condition of ZCS and ZVS. In this mode, current of  $i_{1b} + i_{2b}$  flows to  $V_1$ . The following two differential equations are given by the equivalent circuit of state b shown in Fig.5.

$$V_0 = -r_0 i_{2b}(t) - 2r_T i_{2b}(t) + 2v_T - \frac{r_L}{2} i_{2b}(t) - \frac{L}{2} \frac{di}{dt} i_{2b}(t) + v_M(t) - r_1 i_{2b}(t) - r_1 i_{1b}(t) + V_1 \quad (8)$$

$$V_1 = 2r_D i_{1b}(t) - 2v_D + \frac{r_L}{2} i_{1b}(t) + \frac{L}{2} \frac{di}{dt} i_{1b}(t) + v_M(t) + r_1 i_{1b}(t) + r_1 i_{2b}(t) \quad (9)$$

The default values of  $i_{1b}$  and  $i_{2b}$  are set as  $I_2$ . The Laplace transforms of both Eqs. (8) and (9) are used to obtain Eqs. (10) and (11).

$$\frac{V_0}{s} = -r_1 \{I_{1b}(s) + I_{2b}(s)\} - \left( \frac{Ls + r_L}{2} + 2r_T + r_0 \right) I_{2b}(s) + \frac{2v_T}{s} + \frac{LI_2}{2} + V_M(s) + \frac{V_1}{s} \quad (10)$$

$$\frac{V_1}{s} = r_1 \{I_{1b}(s) + I_{2b}(s)\} + \left( \frac{Ls + r_L}{2} + 2r_D \right) I_{1b}(s) - \frac{2v_D}{s} - \frac{LI_2}{2} + V_M(s) \quad (11)$$

Since  $i_{1b} = i_{2b}$ , Eq. (12) is obtained from Eqs. (10) and (11).

$$I_{1b}(s) = I_{2b}(s) = \frac{2V_1 - V_0 + 2(v_T + v_D) + LI_2 s}{Ls \left( s + \frac{r_L + 2(r_T + r_D) + r_0 + 4r_1}{L} \right)} = \frac{\frac{V_{1b}}{r_b} - \frac{V_{1b} - I_2}{r_b}}{s + \frac{r_b}{L}} \quad (12)$$

Here, Eq. (13) is obtained from the following formulas:

$$r_b = r_L + 2(r_T + r_D) + r_0 + 4r_1, \\ V_{1b} = 2V_1 - V_0 + 2(v_T + v_D)$$

$$i_{1b}(t) = i_{2b}(t) = \frac{V_{1b}}{r_b} - \left( \frac{V_{1b}}{r_b} - I_2 \right) e^{-\frac{r_b}{L} t} \quad (13)$$

Further, when the current is defined as zero at time  $T_1 + T_2$ , Eq. (14) is obtained from Eq. (13).

$$e^{-\frac{\pi r_b T_2}{\omega L T}} = 1 - \frac{r_b}{V_{1b}} I_2 \quad (14)$$

## 3) State c ( $t = T_1 + T_2 \sim T$ )

The magnetic energy of leakage inductance diminishes when  $t = T_1 + T_2$ . The current flowing to diodes of  $S_1$  is turned to flow through IGBT of  $S_1$  under the condition of ZCS and ZVS. The following two differential equations are given by the equivalent circuit of state c shown in Fig.5.

$$V_0 = -r_0 i_{2c}(t) - 2r_D i_{2c}(t) - 2v_D - \frac{r_L}{2} i_{2c}(t) - \frac{L}{2} \frac{di}{dt} i_{2c}(t) + v_M(t) - r_1 i_{2c}(t) - r_1 i_{1c}(t) + V_1 \quad (15)$$

$$V_1 = r_1 i_{1c}(t) + 2r_T i_{1c}(t) + 2v_T + \frac{r_L}{2} i_{1c}(t) + \frac{L}{2} \frac{di}{dt} i_{1c}(t) + v_M(t) + r_1 i_{2c}(t) \quad (16)$$

The default values of  $i_{1c}$  and  $i_{2c}$  are set as zero. The Laplace transforms of both Eqs. (15) and (16) are used to obtain Eqs. (17) and (18).

$$\frac{V_0}{s} = -r_1 \{I_{1c}(s) + I_{2c}(s)\} - \left( \frac{Ls + r_L}{2} + 2r_D + r_0 \right) I_{2c}(s) - \frac{2v_D}{s} + V_M(s) + \frac{V_1}{s} \quad (17)$$

$$\frac{V_1}{s} = r_1 \{I_{1c}(s) + I_{2c}(s)\} + \left( \frac{Ls + r_L}{2} + 2r_T \right) I_{1c}(s) + \frac{2v_T}{s} + V_M(s) \quad (18)$$

Since  $i_{1c} = i_{2c}$ , Eq. (19) is obtained from Eqs. (17) and (18).

$$I_{1c}(s) = I_{2c}(s) = \frac{2V_1 - V_0 - 2(v_T + v_D)}{Ls \left( s + \frac{r_L + 2(r_T + r_D) + r_0 + 4r_1}{L} \right)} = \frac{\frac{V_{1c}}{r_b} - \frac{V_{1c}}{r_b}}{s + \frac{r_b}{L}} \quad (19)$$

Here, Eq. (20) is obtained from the following formulas:

$$r_b = r_L + 2(r_T + r_D) + r_0 + 4r_1,$$

$$V_{1c} = 2V_1 - V_0 - 2(v_T + v_D)$$

$$i_{1c}(t) = i_{2c}(t) = \frac{V_{1c}}{r_b} \left( 1 - e^{-\frac{r_b t}{L}} \right) \quad (20)$$

Further, when the current is defined as  $I_1$  at time  $T_1$ , Eq. (21) is obtained from Eq. (20).

$$I_1 = \frac{V_{1c}}{r_b} \left( 1 - e^{-\frac{\pi r_b (1-D)}{\omega L}} e^{\frac{\pi r_b T_2}{\omega L T}} \right) \quad (21)$$

### B. Numerical calculations of AC output current waveforms

Using the values of  $I_1$  and  $I_2$ , which are derived from Eqs. (7), (14) and (21), Eqs. (22) and (23) can be obtained.

$$I_1 = \frac{\frac{V_{1a}}{r_a} \frac{r_b}{V_{1b}} \left( 1 - e^{-\frac{\pi a D}{\omega L}} \right) e^{-\frac{\pi b (1-D)}{\omega L}} + 1 - e^{-\frac{\pi b (1-D)}{\omega L}}}{\frac{r_b}{V_{1c}} + \frac{r_b}{V_{1b}} e^{-\frac{\pi a D}{\omega L}} e^{-\frac{\pi b (1-D)}{\omega L}}} \quad (22)$$

$$I_2 = \frac{\frac{V_{1a}}{r_a} \frac{r_b}{V_{1c}} \left( 1 - e^{-\frac{\pi a D}{\omega L}} \right) + \left( 1 - e^{-\frac{\pi b (1-D)}{\omega L}} \right) e^{-\frac{\pi b D}{\omega L}}}{\frac{r_b}{V_{1c}} + \frac{r_b}{V_{1b}} e^{-\frac{\pi a D}{\omega L}} e^{-\frac{\pi b (1-D)}{\omega L}}} \quad (23)$$

We obtained AC output current ( $i_1$ ) through numerical calculations by substituting parameters listed in Table 1 into Eqs. (22) and (23). Fig.7 shows the waveform in pattern (a) in power running mode. Identical analysis was carried out for patterns (b) and (c), to obtain  $i_1$  by changing the value of  $V_1$ , as shown in Figs.8 and 9.

## IV. EXPERIMENTAL RESULTS

We constructed a prototype of the proposed dc-dc converter, with the following specifications: rated output capacity  $P_o = 1\text{kW}$ , rated voltage at low-voltage side  $V_1 = 160\text{V}$ , and rated voltage at high-voltage side  $V_0 = 320\text{V}$ . Using the prototype, its conversion efficiency was evaluated by testing under the control of an open-loop system.

### A. Conversion efficiency characteristics of proposed dc-dc converter

Figs.10 and 11 show the conversion efficiency of the proposed dc-dc converter in power running mode, in the case that power source voltage (input side) was changed

Table 1 Circuit symbols and parameters

IGBT threshold voltage	$v_T$	1.0V
Diode threshold voltage	$v_D$	0.7V
IGBT on-resistance	$r_T$	50m $\Omega$
Diode on-resistance	$r_D$	110m $\Omega$
Total resistance of transformer	$r_L$	100m $\Omega$
Internal resistance of low voltage source	$r_i$	1m $\Omega$
Internal resistance of high voltage source	$r_o$	1m $\Omega$
Leakage inductance of transformer	$L$	220 $\mu\text{H}$
Voltage of transformer	$v_M$	160V = $V_0/2$
Switching frequency	$f$	20kHz
Direct voltage source in low voltage side	$V_1$	160V
Direct voltage source in high voltage side	$V_0$	320V

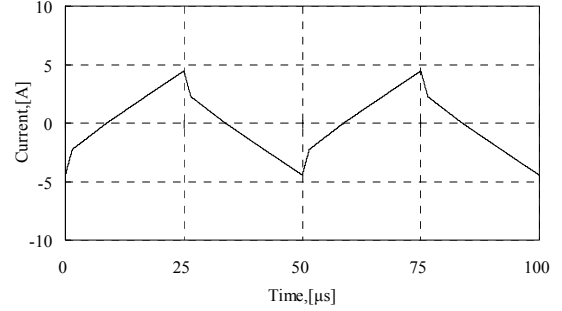


Fig.7. AC output current ( $i_1$ ) in pattern (a) in power running mode. (input voltage 192V, output power 600W)

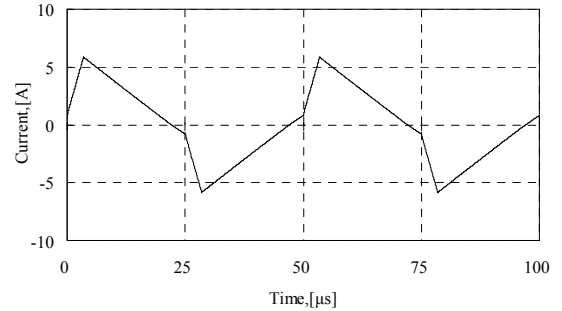


Fig.8. AC output current ( $i_1$ ) in pattern (b) in power running mode. (input voltage 128V, output power 370W)

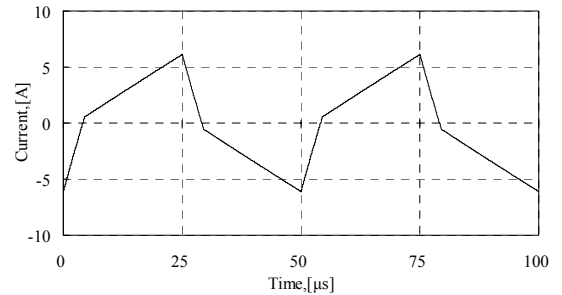


Fig.9. AC output current ( $i_1$ ) in pattern (c) in power running mode. (input voltage 192V, output power 1kW)

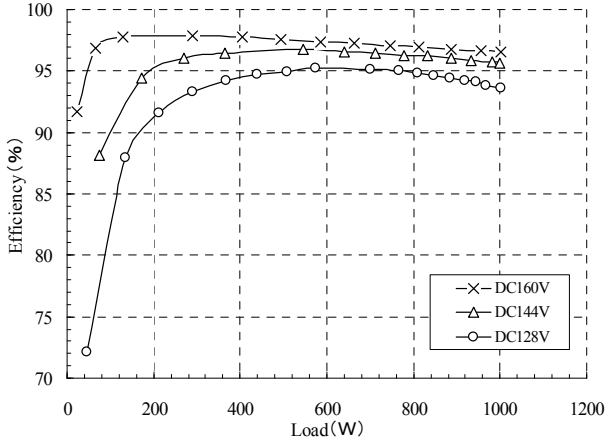


Fig.10. Conversion efficiency in power running mode.  
( $V_i = 160V -10\%, -20\%$ )

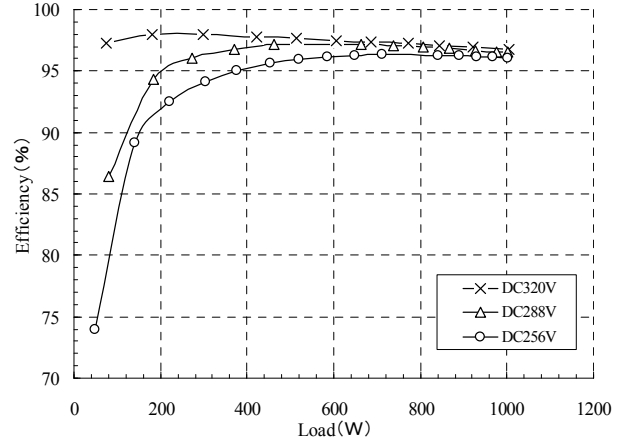


Fig.12. Conversion efficiency in power regenerative mode.  
( $V_o = 320V -10\%, -20\%$ )

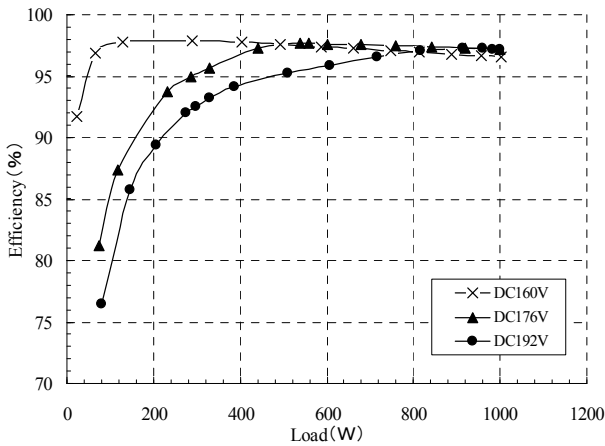


Fig.11. Conversion efficiency in power running mode.  
( $V_i = 160V +10\%, +20\%$ )

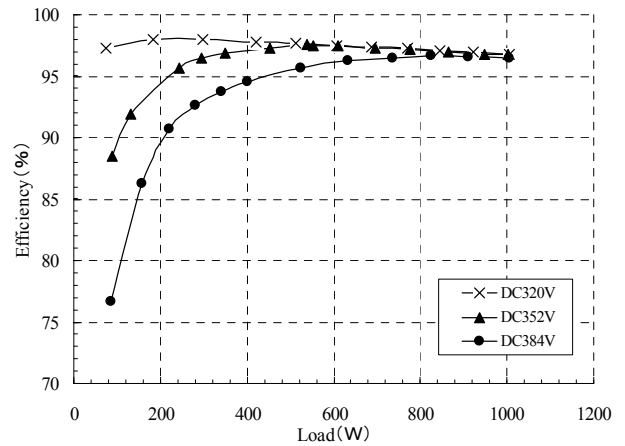


Fig.13. Conversion efficiency in power regenerative mode.  
( $V_o = 320V +10\%, +20\%$ )

by  $\pm 10\%$  and  $\pm 20\%$ , respectively. Power consumed by control source was not included in the conversion efficiency calculation. Figs.12 and 13 show conversion efficiency in power regenerative mode. IGBT were used as switching elements that were incorporated into the converters. IGBT were connected to fast recovery diodes in reverse parallel. Ferrite was used as the core material for the high frequency transformer, which incorporated a mechanism to enfold leakage inductance. As a result of evaluation testing, at the rated input/output voltage with the rated output of 1kW, conversion efficiencies of 96.6% in power running mode, and 96.8% in power regenerative mode were achieved. In the half load region, 97.6% was obtained in power running mode, and 97.7% in power regenerative mode. In all cases, high conversion efficiency was achieved.

We gave particular attention to the following two issues:

- 1) At the rated load, the smaller the input voltage is, the lower the conversion efficiency becomes.

Along with an increase in the current of the converter on the low-voltage side, there are increases in switching loss (at the time of turn off),

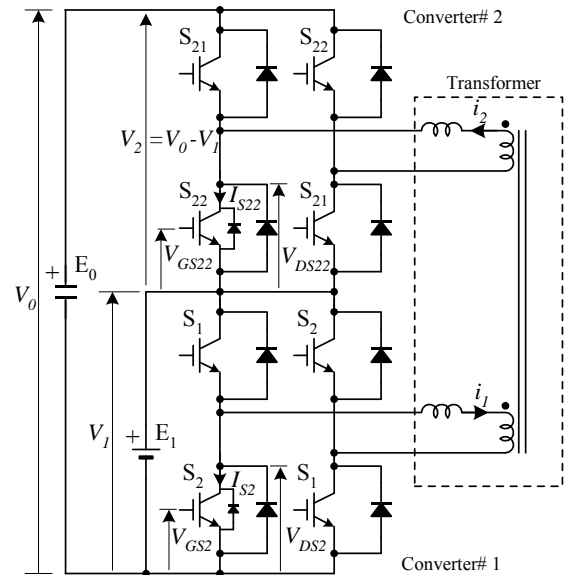


Fig.14. Measurement points for waveforms of current, voltage and output current of the proposed dc-dc converter.

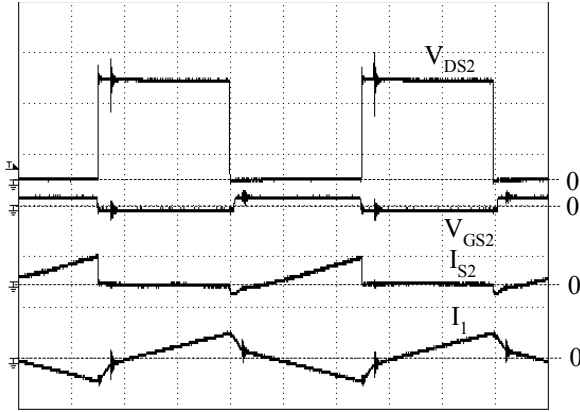


Fig.15. Waveforms of current, voltage and output current ( $i_1$ ) of  $S_2$  (DC input 192V, output 600W in power running mode)

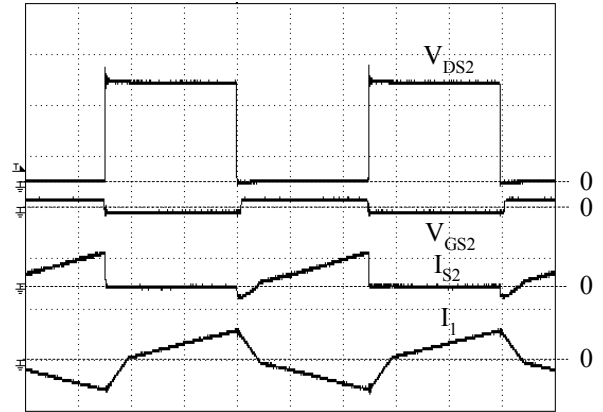


Fig.17. Waveforms of current, voltage and output current ( $i_1$ ) of  $S_2$  (DC input 192V, output 1kW in power running mode)

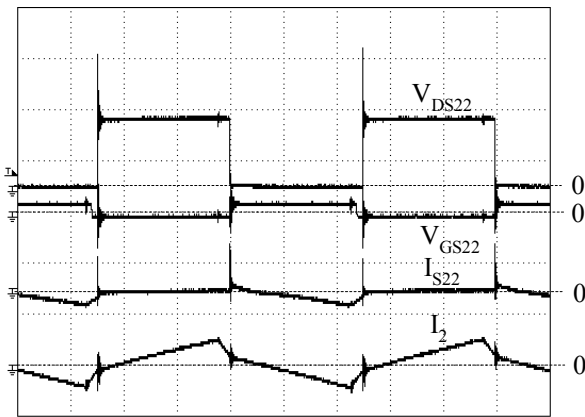


Fig.16. Waveforms of current, voltage and output current ( $i_2$ ) of  $S_{22}$  (DC input 192V, output 600W in power running mode)

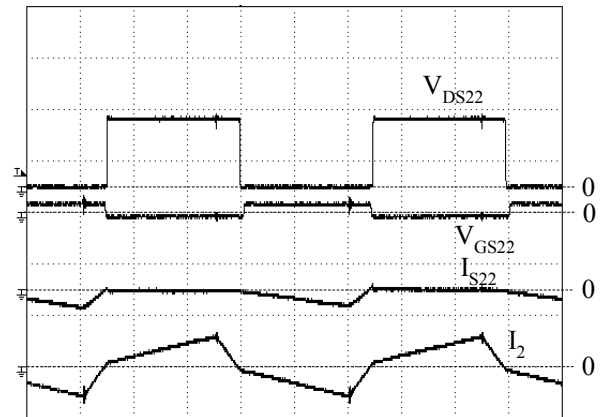


Fig.18. Waveforms of current, voltage and output current ( $i_2$ ) of  $S_{22}$  (DC input 192V, output 1kW in power running mode)

conduction loss, and copper loss, resulting in a drop in efficiency.

- 2) During light load, when the voltage difference between  $V_1$  and  $V_2$  becomes larger, the conversion efficiency drop becomes larger.

Since  $i_1 = i_2$ , the load of converter, having lower voltage as a result of  $V_0$  shared, becomes small. Thus, when voltage difference between  $V_1$  and  $V_2$  becomes larger, the load of either converter becomes smaller. This results in an expansion of the region range in which the hard-turn-on phenomenon occurs.

#### B. Waveforms of current, voltage and power output of converter

Fig.14 indicates measurement points for waveforms of current, voltage and output current ( $i_1$ ) of the proposed dc-dc converter. Fig.15 shows these waveforms for  $S_2$  under the condition of DC input 192V and output 600W in power running mode, while Fig. 16 shows waveforms for current, voltage and output current ( $i_2$ ) of  $S_{22}$  under the same conditions. Figs.17 and 18 show those under

conditions of DC input 192V and the rated output 1kW in the same mode, for  $S_2$  and  $S_{22}$  respectively. The waveform of  $i_{S22}$  as shown in Fig.16 indicates that the hard-turn-on phenomenon emerged more during lighter load as compared to that shown in Fig.18, when  $S_{22}$  was turned on (at the time of rise of  $V_{GS22}$ ). Further, a reverse recovery current flowed, which caused DC power source ( $V_2$ ) to short-circuit, resulting in generation of surge current and surge voltage. The waveforms in Figs.15 and 16 were specially produced to emphasize the hard-turn-on phenomenon, while maintaining output voltage ( $V_0$ ) of 320 V, and raising input voltage ( $V_1$ ) up to 192 V, because the hard-turn-on phenomenon cannot be observed under the condition that only a small percent of rated load in the case of  $V_0$  of 320V and  $V_1$  of 160V.

In the case of  $V_1 > V_2$ , waveforms in Figs.15 and 17 show that current ( $i_{S2}$ ) flowing to  $S_2$  was negative when  $S_2$  was turned on (at the time of rise of  $V_{GS22}$ ) whether load was large or small. It was found that current flowed to anti-parallel diodes of  $S_2$ , and  $V_{DS2}$  was clamped by the forward voltage of diodes. Thus, the turn-on of  $S_2$  occurred under the condition of ZVS and ZCS. In the case of the rated load, waveforms in Fig.18 show that the turn-on of  $S_{22}$  also occurred under the condition of ZVS and ZCS, contributing to high conversion efficiency.

The waveforms of output current ( $i_l$ ) shown in Figs.15 and 17 are extremely in good agreement with numerical calculations shown in Figs.7 and 9. This fact shows a valid performance of the proposed dc-dc converter's equivalent circuit, as well as effectiveness of the analysis result derived from the data using the circuit.

## V. CONCLUSION

Through the performance analysis and evaluation test, the authors were able to theoretically clarify the superior conversion efficiency of their proposed bidirectional superposed dual active bridge dc-dc converter. The proposed dc-dc converter has no function to isolate the input and output power circuits, However, there are beneficial characteristics. The output voltage and DC current of power source can be shared by two converters, contributing to downsizing of converter, as well as reduction in power losses of switching elements and transformers. As a result of evaluation testing, in the case of rated output of 1kW, conversion efficiency of 96.6% in power running mode, and that of 96.8% in power regenerative mode were achieved. The future approach will be to carry out a detailed analysis of power losses, and to study the use of transformer core material with a lower loss. In addition, further efforts will be made to resolve conversion efficiency drop resulting from the hard-turn-on phenomenon, aimed at the further improvement of efficiency.

## REFERENCES

- [1] M. H. Kheraluwala, R. W. Gascoigne, D. M. Divan, and E. D. Baumann, "Performance characterization of a high-power dual active bridge dc-to-dc converter," *IEEE Trans. Ind. Appl.*, vol. 27, no. 6, pp. 1294-1301, Nov./Dec. 1992.
- [2] S. Inoue and H. Akagi, "A bidirectional isolated dc-dc converter as a core circuit of the next-generation medium-voltage power conversion system," *IEEE Trans. Power Electron.*, vol. 22, no. 2, pp. 535-542, Mar. 2007.
- [3] Huang-Jen Chiu and Li-Wei Lin, "A bidirectional dc-dc converter for fuel cell electric vehicle driving system," *IEEE Trans. Power Electron.*, vol. 21, no. 4, pp. 950-958, Jul. 2007.
- [4] S. Inoue and H. Akagi, "A bidirectional dc-dc converter for an energy storage system with galvanic isolation," *IEEE Trans. Power Electron.*, vol. 22, no. 6, pp. 2299-2306, Nov. 2007.
- [5] T. Hirose, H. Matsuo, Y. Ishizuka, "Development of an independent type of hybrid power generation system," in *Proc. IEEE International Telecommunications Energy Conf. (INTELEC)*, vol.31, pp. 598-602, Oct. 2009.
- [6] K. Iida, H. Matsuo, T. Hirose, Y. Ishizuka, "A novel bidirectional dc-dc converter with high efficiency and small size ac-link," in *Proc. IEEE International Telecommunications Energy Conf. (INTELEC)*, vol.31, pp. 11-18, Oct. 2009.